J Mol Model (2006) 12: 445–452
DOI 10.1007/s00894-005-0069-8

ORIGINAL PAPER

Rong-Ren Kuang · Feng Qian · Zhong Li · Dong-Zhi Wei

Study on improving the selectivity of compounds that inhibit two PI3Ks (gamma and delta)

Received: 11 January 2005 / Accepted: 2 November 2005 / Published online: 11 January 2006

Abstract A desirable characteristic of PI3K inhibitors is their selectivity. Up to now, there has been no report that describes the 3 D-structure differences between two PI3Ks (δ and γ) and applies them to designing selective compounds. In the present study, we used an approach combining protein-structure modeling, GRID/PCA (Principal Component Analysis) and docking methods to investigate the detail interactions of the two PI3Ks with various chemical groups. At first, we constructed a 3 D-model of the PI3Kδ catalytic subunit with the program Modeller7.0 based on the high resolution X-ray structure of the PI3Kγ catalytic subunit, and then employed GRID and PCA to reveal the most relevant structural and physicochemical differences between the two PI3Ks related to their selectivity. As a result, the analysis unveiled the most important regions on the two PI3Ks that should be taken into account for the design of selective inhibitors. Finally, based on activity data of 10 PI3Kδ-selective compounds, a docking study validated the results of the GRID/PCA method, which suggested that the approach could provide clear guidelines for selective drug design.

Keywords Selectivity · Homology modeling · GRID · PCA · PI3Kγ · PI3Kδ

R.-R. Kuang · F. Qian · D.-Z. Wei (✉)
State Key Laboratory of Bioreactor Engineering,
New World Institute of Biotechnology,
130 Mei-Long Road,
Shanghai, 200237, People's Republic of China
e-mail: dzhwei@ecust.edu.cn
Tel.: +86-21-64252981
Fax: +86-21-64250068

Z. Li
Institute of Pesticides and Pharmaceuticals,
East China University of Science and Technology,
130 Mei-Long Road,
Shanghai, 200237, People's Republic of China

Introduction

Phosphoinositide 3-kinases (PI3Ks) catalyze the phosphorylation of the 3-OH group of phosphatidyl myoinositol (PtdIns) lipids to generate different 3'-phosphorylated lipid products that act as secondary messengers. PI3Ks were found to play important roles in many of biological processes, such as cell survival and proliferation, cell motility and adhesion, cytoskeletal rearrangement and vesicle trafficking [1, 2]. There are three major classes of PI3Ks (Classes I, II and III), based on their sequences and substrate specificities. Class I PI3Ks are further divided into Class IA and IB according to their regulatory subunit. Class IA enzymes (α, β, and δ) have a p85 regulatory subunit containing two SH2 domains and a p110 catalytic subunit, whereas the Class IB enzyme (PI3Kγ) has a p101 subunit, which is required for maximal Gβγ-stimulated formation of PIP_3 [3, 4], and a p110 catalytic subunit.

In the past several years, two PI3Ks (δ and γ) have sparked a great deal of interest among immunologists and pharmaceutical companies. Macrophages and neutrophils from PI3Kγ-knockout mice show reduced motility in vitro and in vivo models of inflammation, as well as an impaired respiratory burst [5–7]. PI3Kγ-deficient mice also show resistance to thromboembolism [8]. On the other hand, the p110δ-mutant mice suggest that PI3Kδ is the principal isomer responsible for B cell antigen receptor-induced PI3K signaling in B lymphocyte [9–11]. Moreover, the defects in peripheral T lymphocyte of p110δ-mutant mice demonstrate that PI3Kδ plays a role in the differentiation and survival of effector and memory T cells [11]. In addition, the lipid products resulting from PI3K activity are elevated in certain tumors [12, 13]. The above facts show that the two PI3Ks play different roles in organisms except for their commonness, hence isomer (γ or δ) -selective inhibitors have attracted more attention. Recently, patents described some PI3K inhibitors, including PI3Kδ-selective compounds [14–16], whose structures and activities on the two PI3Ks are listed in Table 1. However, reports on the selectivity of PI3Ks are not comprehensive. Moreover, no PI3Kγ-selective inhibitor has been reported until now.

Table 1 Chemical structures of PI3Kδ-selective quinazoline derivatives and their activities[a]

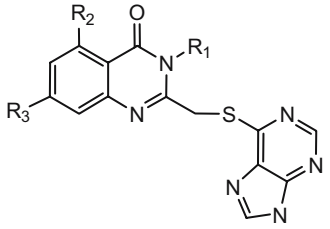

Code	R_1	R_2	R_3	IC50 (μm)		Gamma/ Delta Ratio
				PI3Kδ	PI3Kγ	
D-000	2-Cl-Phenyl	H	H	0.33	7.7	23
D-010	2-Methyl-Phenyl	Cl	H	0.06	0.7	12
D-011	2-F-Phenyl	Cl	H	0.1	1.0	10
D-013	2-Biphenyl	Cl	H	0.05	2.1	42
D-015	2-Cl-Phenyl	F	H	0.21	3.6	17
D-022	2-Cl-Phenyl	H	F	0.8	40	50
D-026	2-Cl-Phenyl	CH_3	H	0.08	1.7	21
D-038	Butyl	H	H	0.9	38	42
D-039	Morpholine	H	H	0.6	60	100
D-047	2-Methoxyphenyl	H	H	0.09	0.5	5.6

[a]Above compound were taken from Reference [16]

Thus it is essential to elucidate the essence of selectivity of the two PI3Ks with an established methodology. To date, six X-ray crystal structures of PI3Kγ complexed with ligands have been reported [17]. The ligands include ATP, wortmannin, Ly294002, quercetin, myricetin, and staurosporine. All these ligands bind to PI3Kγ at the same place. But the X-ray crystal structure of PI3Kδ is still unknown. Sequence comparison of PI3Ks and the complex of ATP/PI3Kγ indicated structural similarity among PI3Ks, which revealed a common catalytic domain of PI3Ks with the most conserved region as its core, and ATP's binding to the conserved region [18]. Thus, we selected this region as the ligand-binding pocket (LBP) of the two PI3Ks.

The objective of this paper is to characterize multivariately the interactions between ligands and the two PI3Ks in order to identify the most selective chemical groups incorporated in novel inhibitors and to exploit the most relevant regions of the two PI3Ks for selective interaction. We used an approach combining protein structure modeling, GRID [19] / PCA [20, 21] and docking methods to investigate the detail interactions of the two PI3Ks with chemical groups. First, taking the crystal structure of PI3Kγ as template, homology modeling and molecular mechanics simulation were used to build the 3 D model of the human PI3Kδ catalytic subunit. Second, the important regions contributing to the two PI3Ks' selectivity were explored with GRID/PCA. Finally, the results of PCA were validated by a molecular docking study on a series of PI3Kδ-selective compounds. The approach gains an advantage over current research methods of isomer-selective PI3K inhibitors. A previous study [16] synthetized hundreds of compounds to search effectively for PI3Kδ-selective inhibitors, but our approach does not require the synthesis of many compounds. In addition, the general results obtained by our approach can be applied to all kinds of PI3K inhibitors. However, those obtained by the traditional method are effective only for a certain type of inhibitors.

Materials and methods

Structure modeling of human PI3Kδ

The amino-acid sequence of human PI3Kδ catalytic subunit was obtained from the Swiss-Prot database [22]. Sequence-homology searches were carried out using the BLAST algorithm [23] against the Protein Data Bank [24]. Then, target-template sequence alignment was created with the CLUSTALW algorithm [25].

The 3 D model of human PI3Kδ catalytic subunit was built up using the crystal structure of the PI3Kγ catalytic subunit (PDB code: 1E7U) as template with the program Modeller7.0 [26]. Each model generated was subjected to various cycles of Modeller, and then the model with the lowest energy was once more subjected to conjugate gradient minimization with the GROMACS 3.0 package. [27] The optimized structure was validated using PROCHECK [28] and ERRAT [29].

Preparation of the PI3Kγ structure

There are six available crystal structures of the PI3Kγ catalytic subunit in the Protein Databank. Here, the PI3Kγ catalytic model was constructed based on the 2.2 Å X-ray crystal structure of the porcine PI3Kγ catalytic subunit with wortmannin, entry code 1E7U. Because the porcine and human enzymes have 95.3% overall sequence homology identity and complete identity in the ATP-binding pocket [17], there is no apparent difference between the two species of PI3Kγ. Water and ligand were removed, and then the enzyme was treated with AutoDockTools for Autodock [30] studies.

Superposition of the ligand-binding pockets

Here we focused on the LBPs of PI3Ks, defined as the collection of amino acids enclosed within a 6 Å radius sphere around ATP. According to Reference [17] eighteen LBP amino acids shown in Table 2, which included residues known to interact with the six above ligands, were chosen. The α-carbons of the eighteen residues were fitted with SwissPdb Viewer [31], resulting in the superposition (shown in Fig. 1) of LBPs of the two PI3Ks. The RMS deviation was 0.39 Å for 18 α-carbons and the largest deviation was 0.54 Å between Asp964, PI3Kγ and Asp911, PI3Kδ.

Table 2 Set of eighteen LBP amino acids for PI3Kγ and PI3Kδ

PI3Kγ	PI3Kδ
Met-804	Met-752
Ala-805	Asp-753
Ser-806	Ser-754
Lys-808	Met-756
Trp-812	Trp-760
Ile-831	Ile-777
Lys-833	Lys-779
Tyr-867	Tyr-813
Ile-881	Val-827
Val-882	Val-828
Ala-885	Ser-831
Thr-886	Asp-832
Lys-890	Asn-836
Asn-951	Asn-898
Met-953	Met-900
Phe-961	Phe-908
Ile-963	Ile-910
Asp-964	Asp-911

Multivariate characterization of the ligand-binding pocket with the GRID force field

The GRID program was used to calculate the energetic interactions between LBPs of the two PI3Ks (targets) and various chemical groups (probes). GRID works by defining a three-dimensional grid of points that contains LBP [19]. At those points throughout the molecule, the interaction of probe with target is calculated from: $E_{total} = [bs]sumE_{LJ} + [bs]sumE_{HB} + [bs]sumE_{Q} + S$, where E_{total}, E_{LJ}, E_{HB}, E_{Q} and S represent overall energy, Lennard-Jones interaction, hydrogen bond interaction, electrostatic interaction and entropic term, respectively. The same calculation is repeated for each point on the grid and for each probe considered. As a result, a collection of three-dimensional matrices, one for each probe-target interaction, is obtained.

Potassium counterions were added to the PI3Kγ structure (1E7U) with the program GREATER in the GRID22 package, while chlorine counterions were added to the PI3Kδ model structure. SwissPdb Viewer was used to visualize and superpose the two PI3Ks and a 22 × 20 × 29 Å grid that enclosed the above residues was selected. The main GRID runs were then carried out with a grid spacing of 1 Å. Non-bonded interaction energies between each protein and the 41 probes shown in Table 3 were calculated.

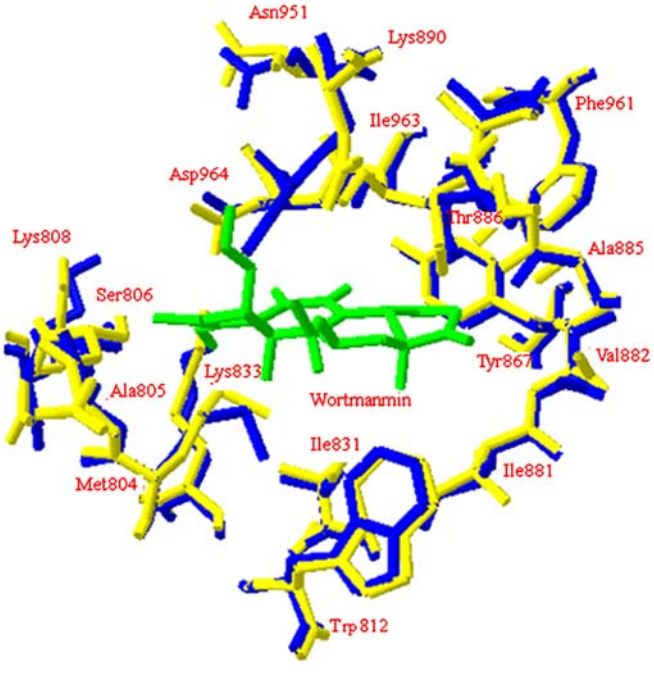

Fig. 1 Superposition of the ligand-binding pockets of PI3Kγ and PI3Kδ. The picture shows the eighteen residues used for the superimposition and all PI3Kγ residues are represented by blue sticks, PI3Kδ residues by yellow sticks and wortmannin by green sticks

Matrix generation and pretreatments

The 3 D-matrices from GRID were rearranged as one-dimensional vectors. One such vector was obtained for each probe-target interaction, and the vectors were used to build a 2 D-matrix X, in which the rows were the probe-target interactions (the objects) and the columns were the variables that described these interactions energetically. Any positive interactions present in the X matrix were set to 0 kcal mol^{-1}. Moreover, all zero variables were cancelled, which focused the work on favorable ligand-target interaction.

Principal component analysis

Information describing the probe-target interaction was contained in the X matrix. In order to simplify the matrix we applied PCA. [20, 21] Briefly, PCA provides an approximation of the matrix X in terms of a score matrix and a loading matrix. The score matrix gives a simple picture of the objects, represented by some uncorrelated new variables (the principal components, PCs) that explain the variation of the X matrix. Score plots reveal the essential data patterns of the objects and here they can display clusters of objects according to the two PI3Ks and probes. The loading matrix and loading plots reveal the relation between the original variables and new PCs and here provide an interpretation in terms of LBP containing the variables most related to each PC. The PCA of the X matrix showed that the variances explained for the first two PCs were 40% and 14%, respectively. Here the two PCs reflected the general variance patterns of the set.

Preparation of ligands

The 10 quinazoline derivatives shown in Table 1 were used in the docking study. Their 3 D-structures were constructed

Table 3 Table of probes used in GRID for the ligand-binding pocket analysis

No.	Code	Description
1	C1=	aromatic CH group
2	C3	methyl group
3	N:	sp^3 nitrogen with lone pair
4	N:=	sp^2 nitrogen with lone pair
5	N–:	anionic nitrogen of tetrazole
6	N:#	sp nitrogen with lone pair
7	N1	amide NH group
8	N1#	sp NH group eg. Acetylene
9	N1=	sp^2 cationic NH group
10	NH=	sp^2 NH group with lone pair
11	N1:	sp^3 NH group with lone pair
12	N1+	sp^2 NH cation
13	N2	amide NH_2 group
14	N2=	sp^2 cation NH_2 group
15	N2:	sp^3 NH_2 group with lone pair
16	N2+	sp^3 cation NH_2 group
17	N3+	sp^3 cation NH_3 group
18	NM3	trimethylammonium cation
19	OC2	ether oxygen atom
20	OES	ester oxygen atom
21	O	carbonyl oxygen atom
22	O::	carboxy oxygen atom
23	ON	nitro oxygen atom
24	O=	phosphate oxygen atom
25	O–	anionic phenolate oxygen atom
26	OS	oxygen of sulfone or sulfoxide
27	O1	aliphatic hydroxyl group
28	OH	phenolic hydroxyl group
29	F	fluorine atom
30	CL	chlorine atom
31	BR	bromine atom
32	I	iodine atom
33	COO–	ionized alkyl carboxyl group (multiatom)
34	AR.COO–	ionized aryl carboxyl group (multiatom)
35	CONH2	alkyl amide (multiatom)
36	AR.CONH2	aryl amide (multiatom)
37	CONHR	alkyl N-alkylamide R.COONHR (multiatom)
38	AR.CONHR	aryl N-alkylamide AR.COONHR (multiatom)
39	AMIDINE	alkylamidine $R.C(NH_2)_2$ (multiatom)
40	AR.AMIDINE	arylamidine $AR.C(NH_2)_2$ (multiatom)
41	M-DIAMINE	m-diaminobenzene (multiatom)

with Cerius2 version 4.8, [32] followed by energy minimization with the Polak-Ribiere and conjugate-gradient methods to a root-mean-square energy gradient of 0.1 kcal (mol^{-1} $Å^2$). The CVFF force field [33] and Gasteiger charges [34] were used throughout.

Molecular docking

Autodock3.0.3 [30] was used for the docking study. It uses a Lamarckian Genetic Algorithm to place ligands into the LBP of a target and then estimates the free binding energy of the ligand-target complex. Normally Autodock provides 10 candidate conformations and the one with the lowest binding energy can be regarded as the bound conformation.

All rotatable bonds of each molecule were considered in the docking process. The atom types, generations and the run numbers for LGA algorithm were properly assigned according to the requirement of the Amber force field. [35] The number of individuals in the population, maximum number of energy evaluations, maximum number of generations and docking runs were set to 150, 3,000,000, 2,700,000 and 10, respectively. Atomic charges were assigned as Kollman all-atom for PI3Kγ and Gasteiger-Marsili for the ligands.

Results and discussion

3 D model of human pi3kδ catalytic subunit

The human PI3Kδ catalytic subunit has 33% sequence identity with that of porcine PI3Kγ, and the crystal structure of the PI3Kγ catalytic subunit is the only experimentally determined structure for PI3Ks. Accordingly, its crystal structure is an appropriate template for modeling the 3 D structure of PI3Ks-family proteins. Because the crystal structures lack the N-terminal region but contain all domains shared with other PI3Ks, [18] here we modeled a fragment of the PI3Kδ catalytic subunit comprising residues 106-1045. The 3 D-model of the PI3Kδ catalytic subunit after energy minimization is shown in Fig. 2. PROCHECK indicated that 95% of the residues of the PI3Kδ model were in the most favorable regions of the Ramachandran plot and the overall main-chain and side-chain parameters were favorable. Moreover, ERRAT demonstrated that the overall quality factor of the model was 83.5, which exceeds its reasonable value, 75.

The overall polypeptide topology of the PI3Kδ catalytic model was similar to that of the PI3Kγ catalytic subunit. It also contained four identifiable homology regions (HRs) with high sequence similarity. These regions were the

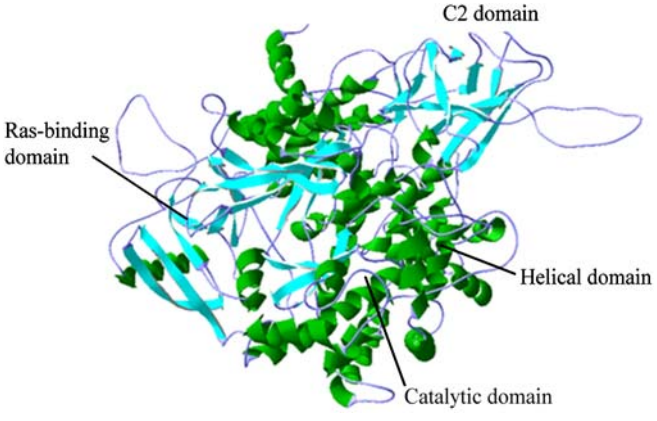

Fig. 2 Ribbon diagram of predicted three-dimensional structure of the human PI3Kδ catalytic subunit

Ras-binding domain (HR4), the C2 domain (HR3), the helical domain (HR2) and the double-lobed catalytic domain (HR1), [18] as shown in Fig. 2. In addition, the catalytic domain of the PI3Kδ model also contained two segments that are essential to catalytic function: the catalytic loop (residues 890-898) and the activation loop (residues 911-935).

A sequence alignment of the two PI3Ks catalytic subunits is shown in Fig. 3, which indicates that residues composing their LBP are relatively conserved and that the two PI3Ks have a common LBP. Moreover, the RMS deviation for superposition of the Cα atoms of the PI3Kδ model with those of PI3Kγ was ~1.03 Å.

Score plots

The score plot for the PC model of the X matrix is shown in Fig. 4. In this plot the points represent single probe (listed in Table 3) -target interactions (objects). The plot shows that PC 1 distinguishes between the two PI3Ks, clustering objects into two groups, while PC 2 ranked the probes. The ability of PC 1 to distinguish between the probe-target interactions involving the two PI3Ks can be explored in several ways. First, variables with high PC 1 loadings indicate regions on the LBP where the probes showed a different behavior when interacting with the two PI3Ks. These regions reveal positions where a chemical group can

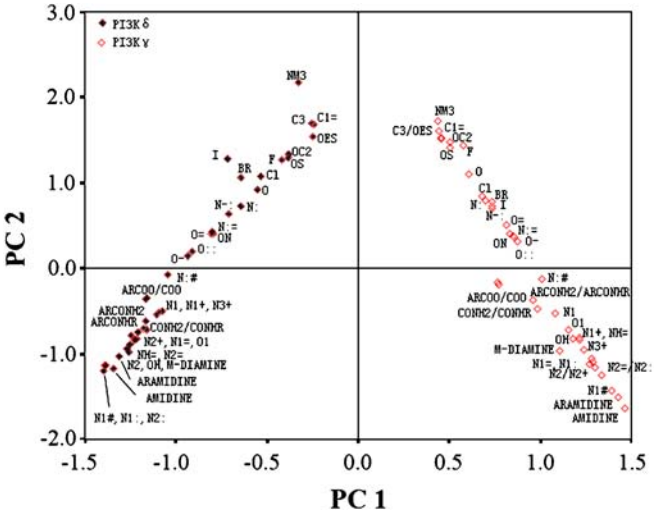

Fig. 4 PC 1 *vs* PC 2 score plot. The points in this plot represent the objects of the X matrix: the interactions of a given probe with PI3Kγ and PI3Kδ. Filled points (♦) represent probe-PI3Kδ interactions. Open points (◇) represent probe-PI3Kγ interactions

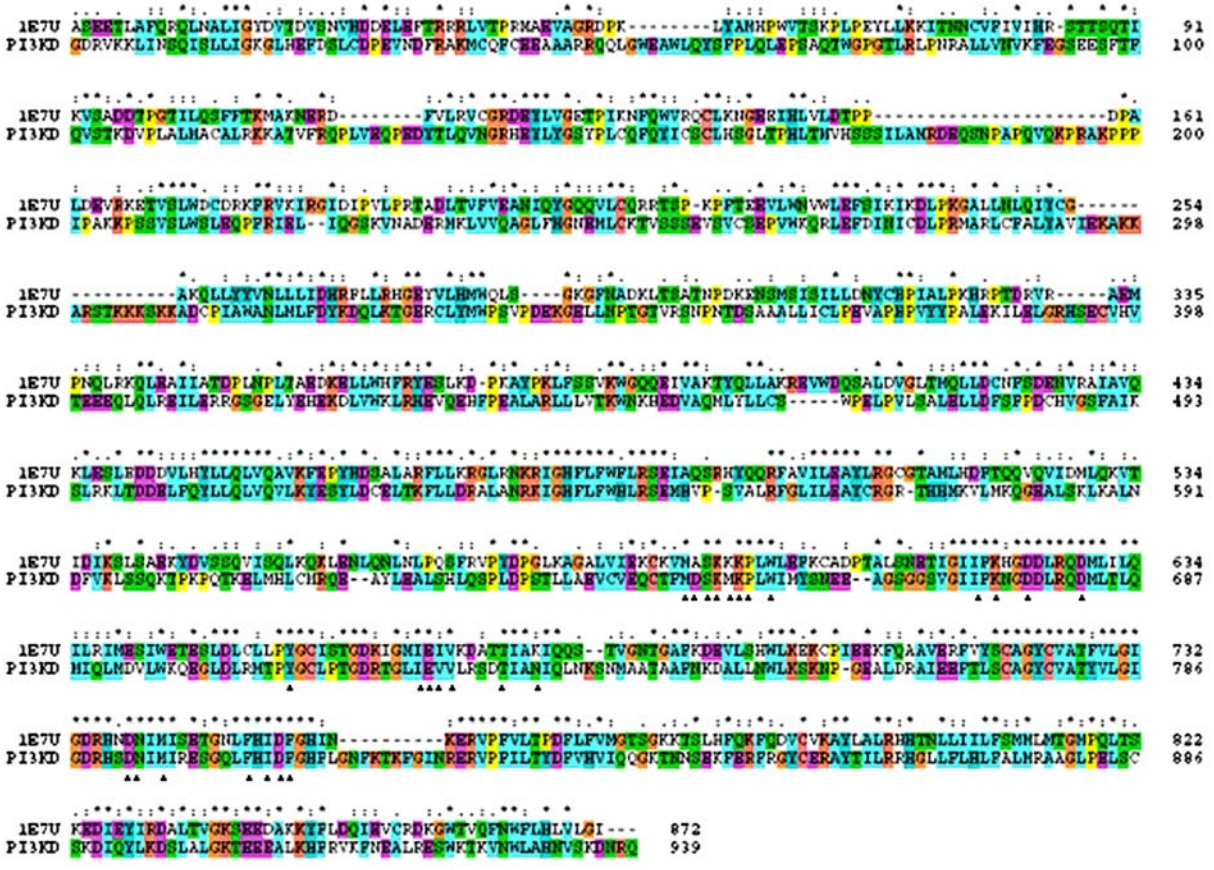

Fig. 3 Sequence alignment of the two PI3Ks catalytic subunits generated by CLUSTALW (1.83). In the sequences, an asterisk (*) indicates an identical or conserved residue, a colon (:) indicates a conserved substitution, a stop (.) indicates a semi-conserved substitution, a triangle (▲) indicates a residue forming the ligand-binding pocket

bind loosely with one of the two PI3Ks and tightly with the other. Also, the absolute PC 1 scores are related to the ability of the groups represented to establish selective interactions. Therefore, it would be preferable to insert chemical groups with higher absolute PC 1 scores. On the other hand, PC 2 is related to nonselective ligand-target interactions. This PC ranked the probes according to their ability to interact with the common region of the LBP. Regions with high PC 2 score highlight areas where probes bind with the same strength for the two PI3Ks. There is an inverse relationship between the strength of binding and the PC 2 scores because favorable binding gives negative energies. Accordingly, those probes that bind loosely with the same areas of the two PI3Ks are in the top part of the score plot, while the probes in the bottom part of the plot interact strongly with the same areas. Further, the points stretched from the top of the score plot to the bottom, which demonstrate that the probes interact strongly with the same regions of the two PI3Ks, are interesting in terms of selectivity.

In short, selective probes are found in the bottom part of Fig. 4 and have high absolute PC 1 scores and negative PC 2 scores. For instance, when designing a novel compound, groups such as sulfone and ether (represented by probe OS and OC2 in Table 3, respectively) are not useful for improving selectivity because of their low absolute values for PC 1, shown in Fig. 4. Furthermore, they cannot increase the nonspecific affinity of compounds due to their positive values of PC 2 in their interaction with both PI3Ks. Instead, groups represented by probes in the bottom part of Fig. 4 (e.g. primary acetylene, N1#), when properly located on the LBP, can strengthen the selectivity of interaction toward both PI3Ks. Moreover, groups with negative PC 2 scores can enhance the nonspecific affinity of compounds.

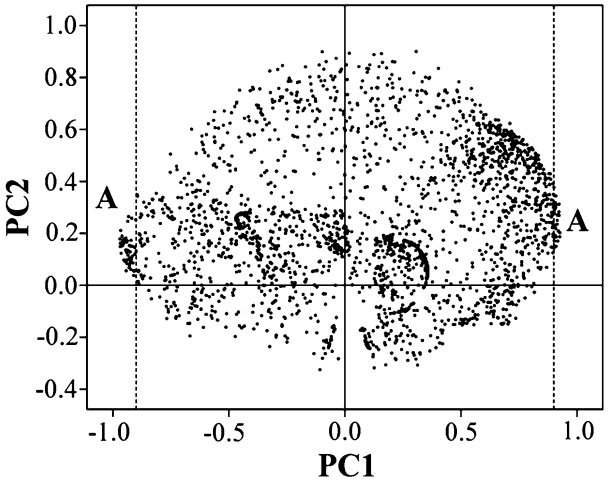

Fig. 5 PC 1 *vs* PC 2 loading plot. The points in this plot represent the variables of the X matrix: the positions in the grid space. The dotted lines define the areas (A) in the plot

Table 4 Main regions involved in selective ligand recognition

Name	Neighboring residues in PI3Kγ	Neighboring residues in PIK3δ	Loadings for PC 1
1	Met-804, Ala-805	Met-752, Asp-753	>0.92
2	Ile-881, Val-882, Ala-885	Val-827, Val-828, Ser-831	>0.92
3	Thr-886	Asp-832	>0.92
4	Lys-890	Asn-836	>0.92
5	Ser-806, Lys-807, Lys-808	Ser-754, Lys-755, Met756	<–0.92

Two-dimensional loading plots

Figure 5 shows a loading plot of the PCA model. In this plot the points describe the contribution to PCs of each position in the selected grid (variables). From the above discussion, the horizontal axis represents PC 1 loadings and, the greater the horizontal spread of a point, the more relevant is the corresponding position to discrimination between the two PI3Ks. The vertical axis represents PC 2 loadings. From the loading plot, we can distinguish one type of positions (A area in Fig. 5) on the LBP that have high absolute PC 1 loading values and intermediate PC 2 loadings. According to our previous interpretation, these probes establish strong selective interactions at these positions, where adequate chemical groups would induce the selectivity of ligands.

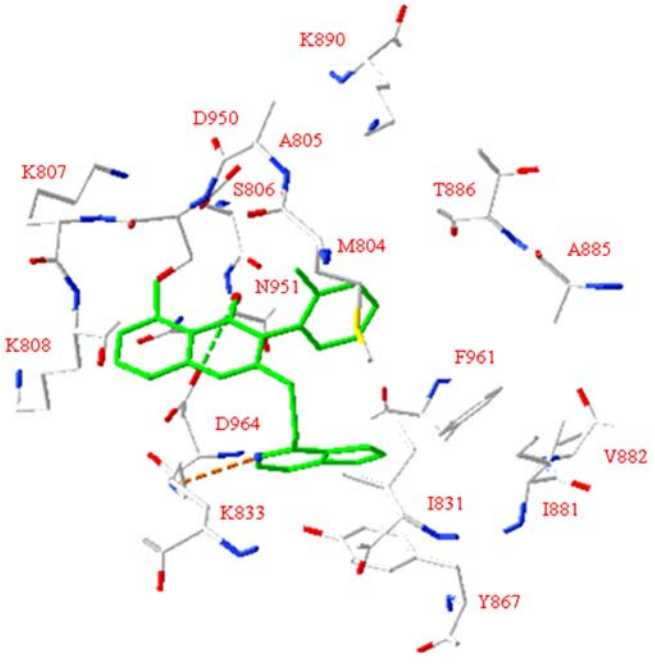

Fig. 6 Three-dimensional structural model of the main interactions between compound D-010 (green) and the ligand-binding pocket of PI3Ks

Regions Involved in Ligand Discrimination

The loading plot was useful for discovering regions involved in ligand discrimination. Hence, by selecting the appropriate PC 1 level, it was possible to display the most relevant regions to selective binding. These regions had an obvious interest for the design of novel compounds, as a proper chemical group in the regions would lead to enhanced selectivity.

From analysis of the loading plot, contour levels of −0.92 and 0.92 were chosen. Lower levels would produce too-confused regions, but a higher level might eliminate some important variables. According to corresponding positions of points in A area, we focused on several main regions in the LBP that were involved in selective ligand recognition. Residues associated with each region were listed in Table 4. As a result of the negative sign assigned to favorable interaction, the loading signs were somewhat inverted. In the regions with negative loadings, the interactions were favorable, with PI3K in the positive part of the score plot and vice versa. This explained why the positive points in the loading plot highlighted regions where chemical groups interact selectively with PI3Kδ, while the negative ones highlighted regions where chemical groups interact selectively with PI3Kγ. The regions shown in Table 4 were attained by comparing their loadings for PC 1 but not the interactions, so their meaning was directly bound to the selectively of the ligand-PI3K interaction.

Regions Contributing to Selectivity of PI3Kδ

Within the LBP of both PI3Ks, there existed six different residues between the two PI3Ks: Ala805, Lys808, Ile881, Ala885, Thr886, Lys890 in PI3Kγ and Asp753, Met756, Val827, Ser831, Asp832, Asn836 in PI3Kδ. The loading plot indicated that they were involved in strong selective ligand–target interaction. As shown in Table 4, the first four regions with positive loadings for PC 1 favorably interacted with PI3Kδ-selective inhibitor. Region 1 enclosed positions where probes can form hydrogen bond and salt bridge with the carboxylic side chain of Asp753, PI3Kδ, with no such residue in PI3Kγ. The introduction of groups binding to Asp753, PI3Kδ would lead to more selective inhibitor toward PI3Kδ. Region 2 was located nearby residues Ile881 and Ala885, PI3Kγ. The selective region derived from the substitution by Val827 and Ser831, PI3Kδ. Residue Ile881, PI3Kγ has more steric hindrance than Val827, PI3Kδ, and probes can form hydrogen bond with the hydroxyl side chain of Ser831, PI3Kδ, while Ala885, PI3Kγ has no such property. For selectivity, it is useful to find group that falls into the region and exploit interactions with the two pairs of residues. Region 3 involved residues Thr886, PI3Kγ and Asp832, PI3Kδ. The main differences of both hydrophilic residues lie in their different size and orientation of the region accessible to favorable interaction. The side chain carboxyl of Asp832, PI3Kδ is exposed more than the hydroxyl of Thr886, PI3Kγ; thus, its side chain carboxyl can more easily form hydrogen bond, and the region also contributed to selectivity of PI3Kδ. Region 4 was nearby Lys890, PI3Kγ and Asn836, PI3Kδ. Lys890, PI3Kγ exhibits side chain shorter than its counterpart in PI3Kδ, which caused ligand to more difficultly interact by hydrogen bond with Lys890, PI3Kγ. The four regions composed a PI3Kδ-selective pocket. In addition, the application of the method to other PI3Ks (γ vs α and δ vs β) also demonstrated the role of the pocket in selectivity of PI3Kδ. Therefore, the pocket was helpful in improving inhibitor selectivity toward PI3Kδ.

Regions Contributing to Selectivity of PI3Kγ

Compared with regions contributing to the selectivity of PI3Kδ, regions toward PI3Kγ are scarce, which is possibly the reason why to date no PI3Kγ-selective inhibitor has been reported in the literature. Here we identified region 5 (shown in Table 4), where chemical groups prefer PI3Kγ to PI3Kδ. It is situated in a hydrophilic pocket and is near residues Ser806, Lys807 and Lys808, PI3Kγ (or Ser754, Lys755 and Met756, PI3Kδ). Selectivity of this region originates from substitution of Lys808, PI3Kγ by Met756, PI3Kδ. Hydrophobic residue Met756, PI3Kδ inevitably undermines hydrophilic interactions in this region. In addition, the amide side chain of Lys808, PI3Kγ can enforce ligand-target interactions by hydrogen bonds and salt bridges. Accordingly, region 5 is interesting for the design of a promising PI3Kγ-selective inhibitor.

Interactions between quinazoline derivatives and PI3Kγ

Autodock may produce several binding conformations for each inhibitor. The conformation with the lowest binding energy was selected as the most probable binding conformation. Thus, the most probable binding conformations of five known PI3K inhibitors (their complexes with PI3Kγ were available) [17] in the test set and ten quinazoline derivatives in Table 1 were attained. As a consequence, Autodock could reproduce their bound conformations in crystal structures very well. The RMS deviations for the heavy atoms were 0.92 Å, 1.2 Å, 1.43 Å, 1.22 Å and 1.31 Å for quercetin, myricetin, wortmannin, staurosporine and Ly290,042, respectively, which indicated that the ability of Autodock3.0 to predict bound conformations of ligands is acceptable.

Docking studies on the above quinazoline derivatives showed that their bound conformations are similar. The binding model for D-010 is shown in Fig. 6 to illustrate the interactions of these derivatives with PI3Ks. The 2-adenine moiety of the quinazoline ring resides in the hydrophobic cluster surrounded by residues Ile879, Tyr867, Ile963 and Met953. The 3-substituted moiety (represented by R_1 in Table 1) interacts with a pocket consisting of residues Met804, Ala805, Ala885, Thr886 and Lys890.

Validation of the GRID/PCA method

The 10 compounds in Table 1 are PI3Kδ-selective inhibitors. [16] According to the table, compounds with a different R1 and the same R2 (and R3) show distinct selectivity towards the two PI3Ks, while those with the same R1 and a different R2 (and R3) are similar in selectivity. In combination with docking studies, this indicates that selectivity of inhibitors lies in their interaction with the selective pocket validated by the GRID/PCA method. Moreover, the distinction of the ten compounds in selectivity can be well explained based on GRID/PCA and docking studies. D-039 has the best selectivity because it includes a more selective group (sp3 NH cation, represented by N1+ in Fig. 4). The biphenyl of D-015 and butyl of D-038 fit more deeply into the pocket than D-000, and thus they interact selectively with PI3Kδ relative to D-000. D-000 includes a chlorine atom with higher absolute PC 1 value than the methoxy of D-047 and methyl of D-010, which deciphers their distinction in selectivity. Although D-022 has the same substitute R1 as D-000, it has better selectivity since the fluorine atom (R3) with low selectivity make its chlorine phenyl moiety fit better into the selective pocket. The consistency between the results of the GRID/PCA method and experiments proved the reasonableness of the method and the results can be used for selective drug design.

Conclusion

Homology modeling and molecular mechanics have been used to build up a 3 D model of the PI3Kδ catalytic subunit. Based on the resulting model and the crystal structure of the PI3Kγ catalytic subunit, we have investigated the detailed interactions between the two PI3Ks and various chemical groups with the GRID/PCA method. The results, which have been validated by docking studies on ten PI3Kδ-selective compounds, provide a satisfactory explanation for their distinct selectivity. This indicates the reasonableness of the GRID/PCA method. Meanwhile, the approach revealed some potentially selective chemical groups and the most interesting regions that interact selectively with ligands and thus provide guidelines for selective drug design.

Acknowledgements We gratefully acknowledge financial support from the National Natural Science Foundation of China (No.30171088), Shanghai Key Disciplinary Foundation and "863" Project of China (No.2001 AA215261).

References

1. Vanhaesebroeck B, Waterfield MD (1999) Exp Cell Res 253:239–254
2. Stein RC, Waterfield MD (2000) Mol Med Today 6:347–357
3. Stephens LR, Eguinoa A, Erdjument-Bromage H (1997) Cell 89:105–114
4. Krugmann S, Hawkins PT, Pryer N, Braselmann S (1997) J Biol Chem 27:17152–17158
5. Hirsch E, Katanaev V, Garlanda C, Azzolino O, Pirola L, Sozzani S (2000) Science 287:1049–1053
6. Li Z (2000) Science 287:1046–1049
7. Sasaki T, Irie-Sasaki J, Jones RG, Olivera-dos-Santos AJ, Stanford WL, Bolon B, Wakeham A (2000) Science 287:1040–1046
8. Hirsch E, Ornella B, Philippe T, Muriel, L, Ronan C, Florella A, Matthias W (2001) FASEB J 15:2019–2021
9. Clayton E, Bardi G, Bell SE, Chantry D (2002) M J Exp Med 196:753–763
10. Jou ST, Carpino N, Takahashi Y, Roland P, Jyh-Rong C (2002) Mol Cell Biol 22:8580–8591
11. Okkenhaug K, Bilancio A, Farjot G, Priddle H, Sancho S, Peskett E, Pearce W (2002) Science 297:1031–1034
12. Phillips WA, Clair FS, Munday AD, Tomas RJ, Mitchell CA (1998) Cancer 83:41–47
13. Gershtein ES, Shatskaya VA, Ermilova VD, Kushlinsky NE (1999) Clin Chim Acta 287:59–67
14. Sadhu C, Masinovsky B, Dick K, Sowell CG, Sraunton DE (2003) J Immunol 170:2647–2654
15. Foukasn LC, Daniele N, Ktori C (2002) J Biol Chem 277:37124–37130
16. Sadhu C, Dick K, Treiberg J (2001) International patent 0181346 A2
17. Edward H Walker, Pacold ME, Perisic O, Stephens L, Hawkins PT (2000) Mol Cell 6:909–919
18. Djordjevic S, Driscoll PC (2002) TRENDS Biochem Sci 27:426–432
19. Goodford PJ (1985) J MC 28:849–857
20. Joliffe J (1986) Principal Component Analysis. Springer, Berlin
21. Wold S, Esbensen K, Geladi P (1987) Chemom Intell Lab Syst 2:37–52
22. Bairoch A, Apweiler R (2000) Nucleic Acid Res 28:45–48
23. Altschul SF, Madden TL, Schaffer AA, Jinghui Z, Zheng Z, Miller W (1997) Nucleic Acid Res 25:3389–3402
24. Berman HM, Westbrook J, Feng Z, Gilliland G, Weissig H (2000) Nucleic Acid Res 28:235–242
25. Thompson JD, Higgins DG, Gibson TJ (1994) Nucleic Acid Res 22:4673–4680
26. Sali A, Blundell TL (1993) J Mol Biol 234:779–815
27. Lindahl E, Hess B, van der Spoel D (2001) J Mol Mod 7:306–317
28. Laskowski RA, MacArthur MW, Moss DS (1993) J Appl Cryst 26:283–291
29. Colovos C, Yeates TO (1993) Protein Sci 2:1511–1519
30. Morris GM, Goodsell DS, Halliday RS (1998) J Comput Chem 19:1639–1662
31. Guex N, Peitsch MC (1997) Electrophoresis 18:2714–2723
32. Cerius 2 4.8 (1999) Accelrys Inc
33. Dauber-Osguthrope P, Roberts VA, Osguthorpe DJ, Wolff J, Genest M (1988) Proteins 4:31–38
34. Gasteiger J, Marsili M (1980) Tetrahedron 36:3219–3228
35. Weiner SJ, Kollman PA, Case DA, Singh UC, Ghio C, Alagona G, Weiner P (1984) J Am Chem Soc 106:765–773